ACS APPLIED MATERIALS & INTERFACES

Research Article

www.acsami.org

# Highly Sensitive Detection and Removal of Lead Ions in Water Using Cysteine-Functionalized Graphene Oxide/Polypyrrole Nanocomposite Film Electrode

Rajesh Seenivasan,[†] Woo-Jin Chang,*[,‡] and Sundaram Gunasekaran*[,†]

[†]Department of Biological Systems Engineering, University of Wisconsin-Madison, 460 Henry Mall, Madison, Wisconsin 53706, United States

[‡]Department of Mechanical Engineering, University of Wisconsin-Milwaukee, 3200 North Cramer Street, Milwaukee, Wisconsin 53211, United States

Supporting Information

**ABSTRACT:** We synthesized cysteine-functionalized graphene oxide (sGO) using carbonyldiimidazole as a cross-linker via amide and carbamate linkages. The sGO/polypyrrole (PPy) nanocomposite film was grown on the working electrode surface of a screen-printed electrode (SPE) via controlled one-step electrochemical deposition. The sGO/PPy-SPE was used to detect lead ions ($Pb^{2+}$) in water by first depositing $Pb^{2+}$ on the working electrode surface for 10 min at −1.2 V, and then anodic stripping by differential pulse voltammetry (DPV). The DPV signals were linear in the ranges of 1.4−28 ppb ($R^2$ = 0.994), 28−280 ppb ($R^2$ = 0.997), and 280−14 000 ppb ($R^2$ = 0.990) $Pb^{2+}$. The measurable detection limit of the sensor is 0.07 ppb ($S/N$ = 3), which is more than 2 orders of magnitude below the 10 ppb threshold for drinking water set by the World Health Organization. The average removal efficiency of $Pb^{2+}$ deposited on the electrode was 99.2% ($S/N$ = 3), with relative standard deviation (RSD) of 3.8%. Our results indicate good affinity of sGO/PPy nanocomposite to $Pb^{2+}$, which can be used to effectively adsorb and remove $Pb^{2+}$ in water samples. Therefore, sGO/PPy nanocomposite we synthesized is useful for highly sensitive on-site and real-time monitoring of heavy metal ions and water treatment.

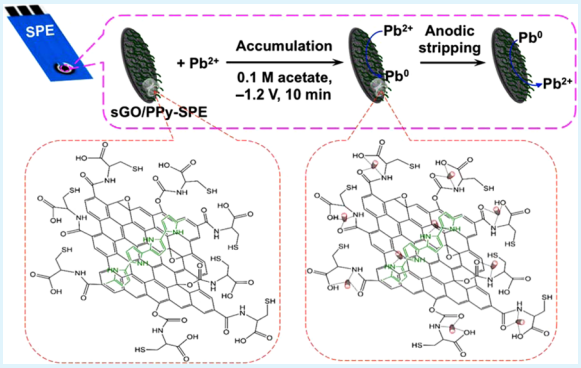


**KEYWORDS:** *cysteine-functionalized graphene oxide, heavy metal, lead ions, differential pulse anodic stripping voltammetry, water treatment*

## INTRODUCTION

Contamination of soil, groundwater, and air with heavy metals, such as lead (Pb), mercury (Hg), cadmium (Cd), copper (Cu), zinc (Zn), etc., is a major environmental problem. Even in trace concentrations, heavy metals present in air, food, and drinking water can bioaccumulate and thus pose major threat to human health.[1−4] Lead is widely recognized as highly toxic and nonbiodegradable; it is a potent neurotoxin and a carcinogen, and causes lung disease, stroke, kidney problems, high blood pressure, etc.[1,3,5−7] World Health Organization (WHO)[6] has established a guideline limiting Pb concentration in drinking water as 10 ppb (μg/L). According to the United States Environmental Protection Agency (U.S. EPA),[7] 10−20% of adults and 40−60% of infants are exposed to Pb via drinking water. Plumlee et al.[4] reported immediate and acute consequence of Pb toxicity in young children through Pb-contaminated soil, water, and food. So, it is essential to detect and carefully monitor the total amount of Pb present in drinking water.

The commonly used analytical methods for the detection of Pb and lead ions ($Pb^{2+}$) include flame atomic absorption spectrometry,[8] inductively coupled plasma (ICP)-atomic emission spectrometry,[9] ICP-optical emission spectrometry,[10] ICP-mass spectrometry,[11] X-ray absorption fine structure spectroscopy combined fluorescence spectrometry,[12] potentiometric ion selective electrode[13] and electrochemical anodic stripping voltammetry.[14,15] Among these, the electrochemical method is very popular because of its many advantages such as high sensitivity, simplicity, reliability, low cost, choice of sensing materials, etc.[16−18]

To date, ethylenediaminetetraacetic acid (EDTA)-bonded conducting polymer,[14] nafion−graphene nanocomposite,[19] L-cysteine (CySH)-functionalized multiwall carbon nanotubes (MWCNT),[20] bismuth (Bi)-nafion-thiolated polyaniline (PANI),[21] polypyrrole (PPy)-carbonaceous nanospheres,[15]

Received: May 5, 2015
Accepted: July 6, 2015
Published: July 6, 2015





DOI: 10.1021/acsami.5b03904
ACS Appl. Mater. Interfaces 2015, 7, 15935−15943

PPy-reduced graphene oxide (rGO) nanocomposites,[22] L-aspartic acid-CySH-gold nanoparticles (AuNP),[23] cysteamine-functionalized graphene,[24] CySH-AuNP-single-walled carbon nanotubes (SWCNT),[25] graphene-carbon nanosheet,[26] graphene oxide (GO),[27] AuNP-graphene-CySH-Bi,[28] and CySH-rGO,[29] have been used to modify working electrodes for sensing heavy metal ions by electrochemical anodic stripping voltammetry. It has been noted that flexible graphene oxide (GO)-PANI and graphene-PANI hybrid offer remarkable combination of excellent electrochemical performance and biocompatibility.[30] Choi and Jang[31] reported that porous carbon materials and their derivatives combined with PPy enhance the adsorption of heavy metal ions from water.

Further, high affinity by functionalized nanomaterials/conducting polymer nanocomposite is a reliable approach to enhance the accumulation of target metal ions on electrode surface for electrochemical detection of heavy metals. Morton et al.[20] designed CySH-functionalized MWCNT-modified glassy carbon electrode (GCE) as a sensor to improve preconcentration and detection of $Pb^{2+}$ and copper ions ($Cu^{2+}$). Tolani et al.[32] synthesized the CySH-modified polymer nanowires to circumvent the drawbacks of other materials used for effective removal of heavy metal ions. For example, ion-exchange resins lack the selectivity to target metal ions, weak binding ability, toxicity from crown ether compounds, and biopolymers are costly and biodegradable. Zhao et al.[22] reported that rGO/PPy is a good sensing material for selective adsorption of mercury ions ($Hg^{2+}$) in the presence of other metal ions, such as $Pb^{2+}$, $Cd^{2+}$, $Cu^{2+}$, and $Zn^{2+}$. The interaction between nitrogen from PPy and $Hg^{2+}$ via affinity enables the selective detection of $Hg^{2+}$. Wang et al.[23] developed L-aspartic acid-CySH self-assembled AuNP-modified microelectrode for the simultaneous detection of $Cu^{2+}$ and $Pb^{2+}$. Fu et al.[25] designed CySH self-assembled AuNP/single wall carbon nanotubes (SWCNT) on working electrode surface for the detection of $Cu^{2+}$. Zhu et al.[28] developed AuNP-graphene-CySH composite modified Bi film electrode for simultaneous determination of $Cd^{2+}$ and $Pb^{2+}$ using square wave anodic stripping voltammetry.

Recent reports show that CySH and GO/PPy nanocomposite is a good choice for the detection of $Pb^{2+}$ because CySH binds well with $Pb^{2+}$ through cooperative metal−ligand interaction. In addition, GO/PPy nanocomposite offers large surface area, fast electron transfer rate, increased mass transport rate, enhanced electrocatalytic properties, lower solution resistance, and higher signal-to-noise ratio. Herein, we combine the advantages of high affinity of CySH toward $Pb^{2+}$ and microporous layered structure and good conductivity of PPy. We enhanced the $Pb^{2+}$ detection sensitivity, suitable for real sample analysis, by functionalizing GO with a large number of CySH moieties via simultaneous modification of −COOH and −OH groups. The CySH-functionalized graphene oxide (sGO) and PPy were grown on the working electrode surface of SPE via controlled one-step electrochemical deposition. The long-term stability and ultrahigh sensitivity of sGO/PPy nanocomposite film modified SPE (sGO/PPy-SPE) make it suitable for detecting $Pb^{2+}$ at levels below the 10 ppb limit for drinking water set by the WHO.

## EXPERIMENTAL SECTION

**Materials.** Graphite flakes (+100 mesh) was purchased from Sigma-Aldrich. Pyrrole, L-cysteine, carbonyldiimidazole (CDI), and lead chloride were purchased from Acros Organics. Whatman no. 1 filter paper was purchased from GE Healthcare Life Sciences. All chemicals used were of analytical grade, and otherwise stated were used without further purification. Lead and other metal ions were prepared daily. Milli-Q water (18.2 MΩ.cm) was used for solution preparation and all experiments.

**Synthesis of Cysteine-Functionalized Graphene Oxide.** GO was synthesized from graphite flakes according to the modified Hummers method,[33,34] following which sGO was synthesized via a two-step procedure outlined in Scheme S1 (Supporting Information). Briefly, 24 mg of GO was dispersed in 40 mL of dimethylformamide by bath ultrasonication for 15 min. After that, 0.1 M CDI was added into the above GO solution (0.6 mg/mL) and bath ultrasonicated for 12 h at 60 °C. This solution was centrifuged at 6000 rpm and washed three times with ethanol and deionized water. After that, 5 mM of CySH was added and reacted with constant stirring for 8 h at room temperature. The obtained product was centrifuged at 6000 rpm, washed with ethanol and deionized water thrice and dried at room temperature. The final product was dispersed in deionized water by bath ultrasonication for further use.

**Instruments and Measurements.** UV−vis spectra of GO and sGO dispersed in water were recorded in the 200−700 nm range using PerkinElmer Lamda-25 UV−vis spectrometer. FT-IR spectra of GO, CySH and sGO were recorded in the range of 4000−650 $cm^{-1}$ using PerkinElmer Spectrum-100 FT-IR spectrometer. The morphology of GO and sGO was characterized using transmission electron microscope (Tecnai T-12 Cyro). The elemental composition of synthesized GO and sGO and GO-, sGO-, PPy-, and sGO/PPy-modified SPEs were examined by X-ray photoelectron spectroscopy (XPS) (Thermo Scientific K-Alpha). Deconvolution of all C 1s spectral peaks were performed using Free XPSPEAK 4.1 software. The surface morphologies of the modified and unmodified SPEs were imaged with a LEO-1530 field-emission scanning electron microscope operating at 5 kV. All electrochemical measurements were performed using CHI-660D, a computer-controlled electrochemical analyzer (CHI, USA). A conventional screen-printed three-electrode system (from CHI, USA) consisting of sGO/PPy-modified carbon as working electrode (diameter=3 mm), carbon as counter electrode, and Ag/AgCl as reference electrode was used. Cyclic voltammetry (CV) and Electrochemical impedance spectroscopy (EIS) measurements were carried out for modified and unmodified SPE characterization in 5 mL of 5 mM redox couple; ferricyanide/ferrocyanide ($[Fe(CN)_6]^{3-/4-}$) solution containing 0.1 M KCl with applied potential range from −0.2 to +0.6 V at scan rate of 50 mV/s and frequency range from 0.1 Hz to 100 kHz at open-circuit potential. Differential pulse anodic stripping voltammetry (DPASV) was performed in 100 μL of working solution placed directly on the electrode surface for $Pb^{2+}$ detection at room temperature.

**Fabrication of sGO/PPy Nanocomposite Film-Modified SPE.** The sGO/PPy nanocomposite film was grown electrochemically on the working electrode surface of SPE. The electropolymerization was carried out in $N_2$ gas purged 0.1 M pyrrole, sGO (0.5 mg/mL) and 0.1 M KCl mixture solution using CV technique between −0.2 V and +0.9 V up to 10 complete cycles at scan rate of 50 mV/s. The modified electrode (sGO/PPy-SPE) was washed with deionized water to remove any physically adsorbed nanocomposite film. For comparison, PPy-SPE was also prepared following the above procedure without sGO. The GO- and sGO-modified SPEs were prepared by placing about 3 μL of GO (1 mg/mL) and sGO (0.5 mg/mL) suspensions on the working electrode surface of SPE and drying at room temperature.

## RESULTS AND DISCUSSION

GO affords easy surface modification via covalent grafting due to the presence of carboxyl (−COOH), hydroxyl (−OH), and epoxide (C−O−C) groups on its edge and basal planes.[35,36] On the basis of its structural arrangement, we selected GO as the starting material to synthesize sGO using CDI via amide (from −COOH groups) and carbamate (from −OH groups) linkages. Recent reports show modification of GO with biomaterials, such as CySH, adenine, cystine, etc., by activating


DOI: 10.1021/acsami.5b03904
ACS Appl. Mater. Interfaces 2015, 7, 15935−15943

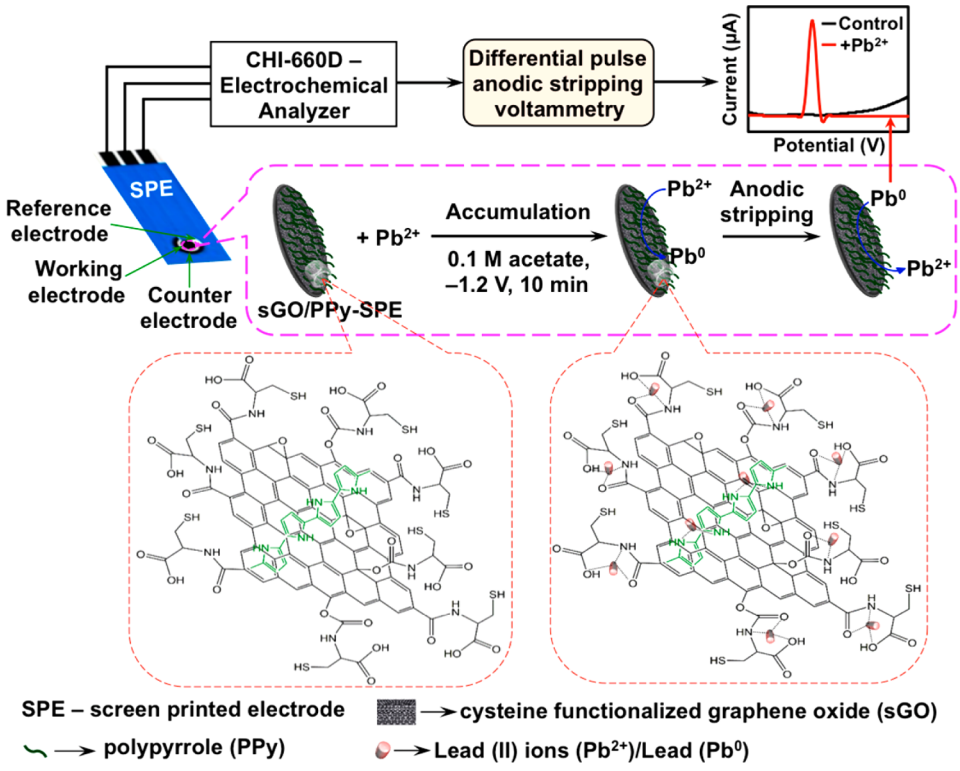


**Figure 1.** Illustration of reactions occurring at the working electrode surface of the SPE (accumulation and stripping of $Pb^{2+}$).

the $-COO^-$ group using 1-ethyl-3-[3-(dimethylamino)propyl]-carbodiimide/*N*-hydroxysuccinimide and *N*,*N*′-dicyclohexylcarbodiimide as a cross-linker.[29,37] However, we synthesized sGO by activating the −COOH, and −OH groups simultaneously using CDI to obtain large number of CySH moieties on the GO surface (see Scheme S1, Supporting Information).

The synthesized sGO and PPy was electrochemically grown on the working electrode surface of SPEs and used for DPASV-based sensing of $Pb^{2+}$ as illustrated in Figure 1. The sGO/PPy film has good electron tunneling properties, large surface area, good conducting ability and high affinity to $Pb^{2+}$. The overall mechanisms of accumulation and anodic stripping of $Pb^{2+}$ during DPASV measurements may be described as follows:[20,38,39]

accumulation

$$(\mathrm{sGO/PPy})_{\mathrm{workingsurface}} + (\mathrm{Pb}^{2+})_{\mathrm{solution}} + 2\mathrm{e}^- \rightarrow (\mathrm{Pb}^0 \cdots \mathrm{sGO/PPy})_{\mathrm{workingsurface}}$$

anodic stripping

$$(\mathrm{Pb}^0 \cdots \mathrm{sGO/PPy})_{\mathrm{workingsurface}} \rightarrow (\mathrm{Pb}^{2+})_{\mathrm{solution}} + (\mathrm{sGO/PPy})_{\mathrm{workingsurface}} + 2\mathrm{e}^-$$

**UV−vis, FT-IR, TEM, and XPS Characterization of Synthesized GO and sGO.** The UV−vis spectrum of GO (Figure S1a, Supporting Information) shows a strong absorption peak at 230 nm corresponding to the $\pi \rightarrow \pi^*$ electronic transitions in aromatic C═C structure and a shoulder at ∼300 nm corresponding to the $n \rightarrow \pi^*$ electronic transitions in carbonyl (C═O) groups.[36,40] After CySH modification of GO, the absorption peak at 230 nm disappeared and no new peak appeared around 270 nm for rGO (Figure S1b, Supporting Information), signifying that the CySH moiety covalently linked with GO surface. Chen et al.[41] reported that CySH used as a reducing agent to synthesize rGO from GO under mild reaction conditions.

The FT−IR spectra offer evidence that CySH is covalently bound to GO (Figure S2, Supporting Information). The spectrum of GO (Figure S2a, Supporting Information) shows the presence of O−H ($\nu_{O-H}$ at 3409 $cm^{-1}$), stretching vibration of C═O ($\nu_{C=O}$ at 1742 $cm^{-1}$) and C−O ($\nu_{C-O}$ at 1375 $cm^{-1}$) in carboxyl groups, aromatic C═C ($\nu_{C=C}$ at 1631 $cm^{-1}$), epoxy C−O ($\nu_{C-O}$ at 1242 $cm^{-1}$) and alkoxy C−O ($\nu_{C-O}$) at 1045 $cm^{-1}$.[42,43] Figure S2b, Supporting Information, shows the asymmetric stretching peak of $-COO^-$ at 1590 $cm^{-1}$ and the symmetric stretching peak of $-COO^-$ at 1394 $cm^{-1}$ in CySH. The $NH_3^+$ stretching peak was observed at ∼3197 $cm^{-1}$ and a weak peak near 2578 $cm^{-1}$ confirms the presence of −S−H group in CySH.[44] The peak at 1729 and 1390 $cm^{-1}$ indicates the presence of carboxyl group ($\nu_{C=O}$ and $\nu_{C-O}$ stretch) in sGO (Figure S2c, Supporting Information). The characteristic of amide I and amide II (C−N stretch and N−H deformation) peaks are seen at 1628 and 1593 $cm^{-1}$,[20,42,43] which imply that the CySH moieties are successfully bound on the GO surface. The transmission electron microscopy (TEM) images of GO and sGO are shown in Figure S3a and b, Supporting Information. The TEM image before CySH modification GO (Figure S3a, Supporting Information) shows the formation a large and thick two-dimensional structure. After CySH modification of GO (Figure S3b, Supporting Information) gives the few nanosheets with fewer of wrinkles.[45] Further, X-ray photoelectron spectroscopy (XPS) results of the synthesized GO and sGO are shown in Figure S4 (details in Supporting Information). The results of wide scan spectral analysis presented in Table S1 (Supporting Information) lists


DOI: 10.1021/acsami.5b03904
ACS Appl. Mater. Interfaces 2015, 7, 15935−15943

the binding energy, elemental identification, atomic composition (%), and ratio of synthesized GO and sGO.

sGO/PPy (Figure S5A, Supporting Information) and PPy (Figure S5B, Supporting Information) films were grown electrochemically on the SPE working electrode surface using CV at scan rate of 50 mV/s. The first complete cycle indicates that the pyrrole monomer oxidation potential began at +0.6 (Figure S5A, Supporting Information) and +0.7 V (Figure S5B, Supporting Information), and the irreversible peaks observed imply nucleation and growth of PPy film.[46] Further, it is seen that the current increased with each subsequent cycle from second to 10th. During electrochemical polymerization, the adhesive PPy film was grown on the sGO surface (perhaps via $\pi-\pi$ stacking interaction and hydrogen bonding) to form a nanocomposite film with good orientation, stability and conducting property on the SPE surface.[22,46]

**Surface Morphology, XPS, and Electrochemical Characterization of Fabricated Electrodes.** The scanning electron microscopy (SEM) images of bare, PPy-, GO-, and sGO/PPy-modified SPEs are shown in Figure 2. Figures 2b and 2d verify that the PPy and sGO/PPy have been successfully grown on the SPE. PPy along with sGO nanosheet is uniformly distributed over the entire carbon working electrode surface of the SPE. This morphology leads to surface area larger than that of bare (Figure 2a) and GO-modified (Figure 2c) SPEs. Figure 2d reveals that the surface of electrochemically grown sGO/PPy nanocomposite film is more porous and uniformly thin than that of the chemically modified graphene-PPy reported by Ye et al.[47] XPS was performed to characterize the elemental identification (C 1s, O 1s, N 1s, S 2p, Cl 2p), atomic composition, and bonding configuration of functional groups in GO-, sGO-, PPy-, and sGO/PPy-modified working surface of SPEs (Figure S6) (details in Supporting Information). The wide scan spectral binding energies, elemental identification, atomic composition (%) and ratio of GO-, sGO-, PPy-, and sGO/PPy-SPEs are shown in Table S2 (Supporting Information).

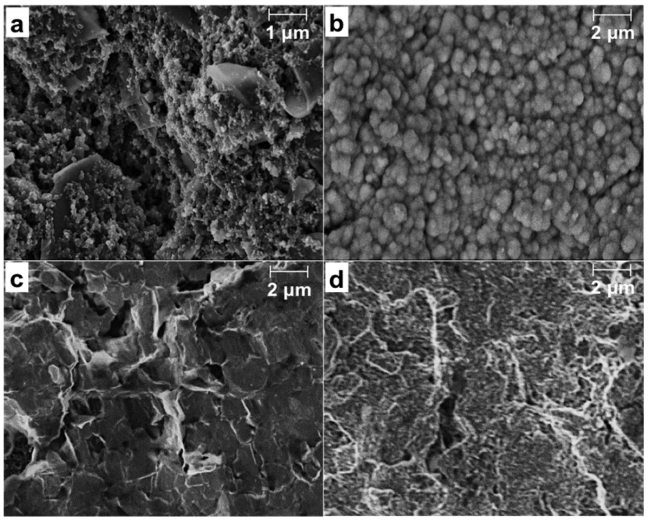


**Figure 2.** SEM images of (a) bare and (b) PPy-, (c) GO-, and (d) sGO/PPy-modified SPEs.

Typical CV responses of bare and GO-, sGO-, PPy-, and sGO/PPy-modified SPEs in 5 mM of redox couple $[Fe(CN)_6]^{3-/4-}$ and 0.1 M KCl solution is displayed in Figure 3A. Figure 3A, curve a shows a quasi-reversible anodic and cathodic peaks of $[Fe(CN)_6]^{3-/4-}$ at the bare SPE surface. The current at GO-SPE decreased more rapidly than at bare SPE (Figure 3A, curve b) due to −COOH, −OH, and C−O−C groups on the edge/basal planes of GO,[36] which block the redox reaction and hinder electron transfer between $[Fe(CN)_6]^{3-/4-}$ and the electrode surface. Figure 3A, curve c exhibits a well-defined redox peak with increases in current at sGO-SPE. In the case of electrochemically polymerized PPy on SPE surface (Figure 3A, curve d), well-defined reversible redox peaks were observed with up to 2-fold increase in current than in sGO-SPE. This result confirms that PPy has good electron tunneling properties and enhances the rate of electron transfer at the electrode surface.[22] After electrochemically growing sGO/PPy on the SPE surface, further increase in current was observed as shown in Figure 3A, curve e. The sGO/PPy-SPE has a good Faradaic redox behavior compared with bare and PPy-, sGO-, and GO-modified SPEs. These results reveal that the sGO/PPy provides good conductivity, large surface area, and better electrochemical catalytic behavior,[22,46] which promote electron transfer rate at the modified electrode surface and improve the sensitivity of $Pb^{2+}$ sensing.

EIS measurements were performed to further investigate the electrode surface characteristics during each step of modification (Figure 3B). In typical Nyquist plots of the EIS spectra, the diameter of semicircle parts at higher frequency range corresponds to electron-transfer-limiting process, and the linear parts at lower frequency range represent diffusion-limiting process.[48] Thus, a large semicircle obtained at high frequency range (Figure 3B, curve a) explains the poor electron

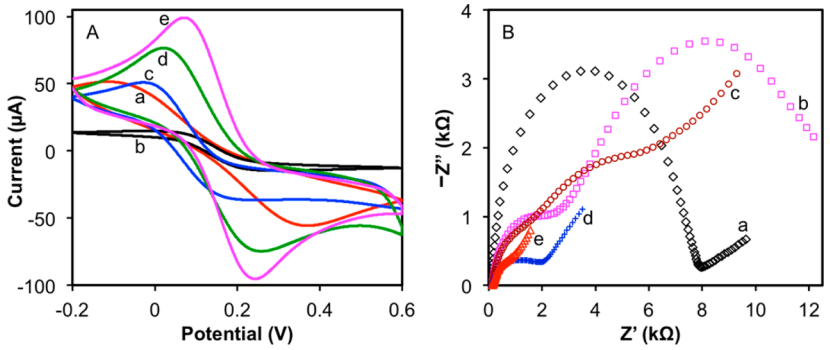


**Figure 3.** (A) Typical cyclic voltammograms of (a) bare and (b) GO-, (c) sGO-, (d) PPy-, and (e) sGO/PPy-modified SPEs in 5 mM $[Fe(CN)_6]^{3-/4-}$ and 0.1 M KCl at scan rate of 50 mV/s. (B) EIS of (a) bare and (b) GO-, (c) sGO-, (d) PPy-, and (e) sGO/PPy-modified SPEs in 5 mM $[Fe(CN)_6]^{3-/4-}$ and 0.1 M KCl.



DOI: 10.1021/acsami.5b03904
ACS Appl. Mater. Interfaces 2015, 7, 15935−15943

transfer reaction of $[Fe(CN)_6]^{3-/4-}$ at the bare SPE. After modified by GO on SPE (Figure 3B, curve b), the charge transfer resistance ($R_{CT}$) value further increased up to 12.17 kΩ compared with that of bare SPE (7.97 kΩ) because the electron transfer reaction is hindered by −COOH, −OH and C−O−C groups in GO. However, sGO-SPE shows two small semicircles with $R_{CT}$ values of 1.56 and 5.2 kΩ (Figure 3B, curve c). With PPy-SPE, the $R_{CT}$ value further decreased to 1.98 kΩ (Figure 3B, curve d), confirming the ability of PPy to promote electron-transfer reaction of $[Fe(CN)_6]^{3-/4-}$. With sGO/PPy-SPE, $R_{CT}$ (0.763 kΩ) decreased even more substantially as noted from the semicircle parts in the Nyquist plots being reduced to almost a straight line (Figure 3B, curve e). These EIS results concur with those obtained with CV.

**Electrochemical Detection of $Pb^{2+}$.** The DPASV measurements were performed using sGO/PPy-SPEs for the detection of $Pb^{2+}$ in 0.1 M sodium acetate-acetic acid (acetate) buffer at pH 5.0 as supporting electrolyte (Figure 4A). After a

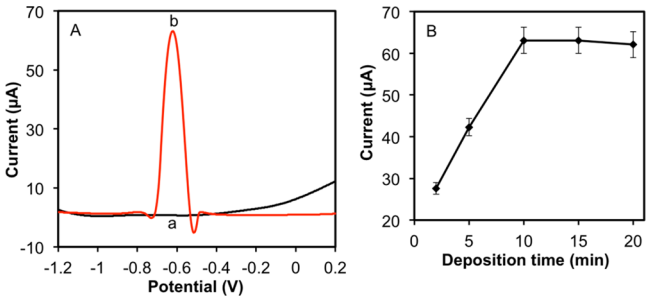


**Figure 4.** (A) DPASV (deposition potential = −1.2 V, deposition time =10 min) results of (a) in the absence and (b) in the presence of 14 ppm $Pb^{2+}$ in 0.1 M acetate buffer (pH 5.0) using sGO/PPy-SPE. (B) Effect of deposition time at deposition potential = −1.2 V on the anodic stripping peaks of 14 ppm $Pb^{2+}$ in 0.1 M acetate buffer (pH 5.0).

preconcentration step performed for effective accumulation of $Pb^{2+}$ on sGO/PPy, 14-ppm analyte solution was placed on the electrode surface and the deposition potential of −1.2 V was applied for 10 min in open circuit condition. Then DPASV measurements were performed by scanning the stripping voltammetric potential from −1.2 to +0.2 V with an increment potential of 4 mV with a pulse amplitude of 50 mV, pulse width of 0.2 s and pulse period of 0.3 s. Well-defined stripping peak of $Pb^{2+}$ is seen at −0.63 V with increase in current. The results confirm that sGO/PPy has good affinity to $Pb^{2+}$, and CySH plays an important role in enhancing the affinity with $Pb^{2+}$ and its accumulation on the working electrode surface of SPE.[20,28]

The effect of electrolytes other than acetate buffer was also studied. The DPASV results for the detection of 14 ppm $Pb^{2+}$ in the following buffers 0.1 M sodium acetate (pH 4.5), 0.1 M HCl (pH 2.0), and 0.1 M phosphate ($NaH_2PO_4/Na_2HPO_4$) (pH 7.0) at their corresponding $Pb^{2+}$ anodic stripping values are 53.4 μA at −0.54 V, 2.89 μA at −0.53 V, and 20.0 μA at −0.7 V, respectively (Figure S7, Supporting Information). Since the highest current response at well-defined anodic stripping peak of $Pb^{2+}$ (63.1 μA at −0.63 V) were obtained in 0.1 M acetate buffer, it was selected for further studies. The deposition time during DPASV was varied from 0 to 20 min. Figure 4B shows the effect of deposition time on the detection of $Pb^{2+}$. The stripping peak at −0.63 V increased at deposition potential of −1.2 V for up to 10 min of deposition, which was chosen as optimal.

The DPASV results obtained with bare and GO-, sGO-, PPy-, and sGO/PPy-modified SPEs for 14 ppm $Pb^{2+}$ ($n$ = 3, triplicates) under the above optimal experimental conditions (Figure S8) show that the maximum anodic peak current response was obtained with sGO/PPy-SPE (63.1 μA at −0.63 V). This is much higher than those obtained with other electrodes: PPy-SPE (28.09 μA at −0.61 V), sGO-SPE (42.44 μA at −0.66 V), GO-SPE (23.45 μA at −0.61 V), and bare SPE (45.18 μA at −0.61 V). The relative standard deviation (RSD) of measurements with sGO/PPy-SPE was 3.0%, which was lower than those with sGO-SPE (RSD = 3.4%), PPy-SPE (RSD = 3.8%), GO-SPE (RSD = 4.7%), and bare SPE (RSD = 5.7%). Thus, the performance of our sGO/PPy-SPE is better than that of sGO-SPE and other $Pb^{2+}$ sensors reported in the literature.[20,29] The PPy-SPE exhibited some value of $Pb^{2+}$ stripping peak, which indicates that −N− in pyrrole ring may have little affinity with $Pb^{2+}$ (see Scheme S1, Supporting Information). This result agrees with that of Zhao et al., who reported that PPy has some affinity with $Pb^{2+}$.[22] The result with sGO-SPE compared with that of GO-SPE indicates that the stripping peak current almost doubled and the potential shifting to higher value, which is attributed to binding of CySH moiety with GO and high affinity with $Pb^{2+}$. The $Pb^{2+}$ stripping peak of bare SPE was higher than those of other electrodes, except sGO/PPy-SPE, because carbon on the working electrode surface of SPE is porous (see Figure 2a).

**Linearity, Sensitivity, and Reproducibility.** Typical DPASV results for $Pb^{2+}$ concentrations from 0.28 to 280 ppb in 0.1 M acetate buffer using sGO/PPy-SPE under optimal deposition and stripping conditions are shown in Figure 5A. Well-defined stripping peaks, with peak currents increasing in proportion to the concentration of $Pb^{2+}$ were observed at −0.63 V. The calibration curves for $Pb^{2+}$ were determined using three linear concentration ranges (Figure 5B−D, line a, blue color) from 1.4 to 28 ppb ($R^2$ = 0.994), from 28 to 280 ppb ($R^2$ = 0.997), and from 280 to 14 000 ppb ($R^2$ = 0.990).

Recent reports show that paper is an excellent medium to deliver samples to the working electrode surface for effective detection of target analytes.[18,49,50] Thus, we investigated the effect of placing a 1 cm × 1 cm paper pad over the SPE and performed $Pb^{2+}$ detection experiments. The results obtained without (line a, blue color) and with (line b, red color) the paper pad show no significant differences (Figure 5B−D). Thus, our system can be used with paper as sample delivering medium. The measurable detection limit of 0.07 ppb of $Pb^{2+}$ we achieved is much lower than previously reported without[20,23,29,51,52] and with paper as delivery matrix,[49,53,54] and the 10 ppb limit for drinking water set by the WHO.[6]

The reproducibility of the sensor was tested using three similarly prepared sGO/PPy-SPEs in 14 ppm $Pb^{2+}$ sample under optimal experimental conditions. The average removal of deposited $Pb^{2+}$ was 99.2% ($S/N$ = 3) with the RSD of 3.8%, which is much lower than previously reported CySH-MWCNT-GCE,[20] L-aspartic acid-CySH self-assembled AuNP-modified microelectrode,[23] and AuNP-graphene-CySH-Bi-GCE.[28] Thus, our sensor exhibits good affinity to $Pb^{2+}$ and affords excellent electroanalytical performance such as wide linear range, high sensitivity, and good reproducibility. Also, the synergistic effect of sGO/PPy film resulted in good electrochemical DPASV-based determination of $Pb^{2+}$ compared with those reported for other sensors (Table S3, Supporting Information). Therefore, the sensing performance of our sGO/PPy is very efficient for practical detection of $Pb^{2+}$.


DOI: 10.1021/acsami.5b03904
ACS Appl. Mater. Interfaces 2015, 7, 15935−15943

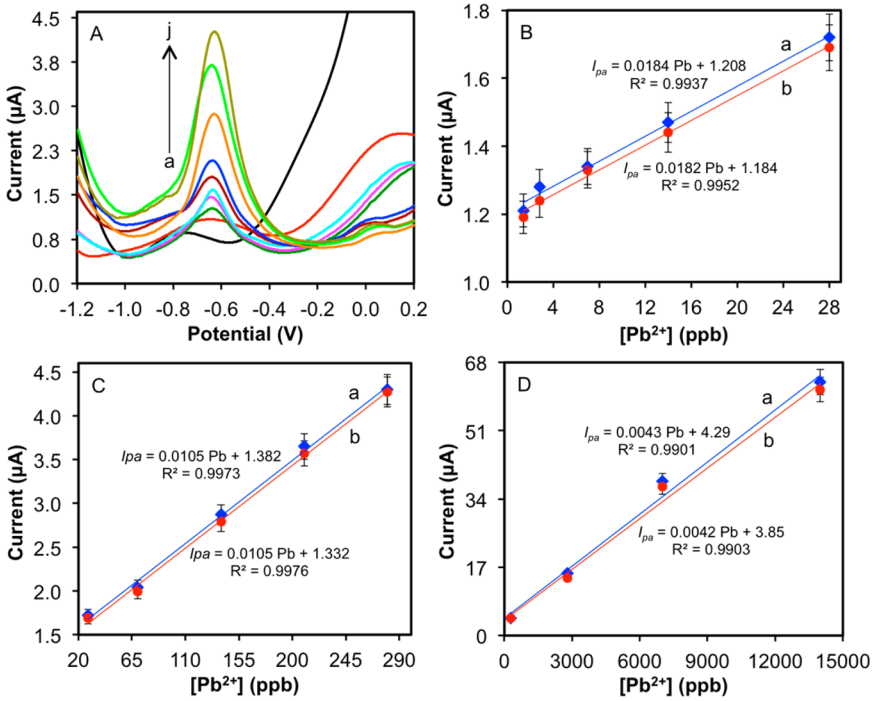


**Figure 5.** (A) DPASV results of various $Pb^{2+}$ concentrations (a–j 0, 0.28, 1.4, 7, 14, 28, 70, 140, 210, and 280 ppb) using sGO/PPy-SPE. Calibration plots between peak current ($I_{pa}$, μA) vs $Pb^{2+}$ (ppb) in three concentration ranges of (B) 1.4–28, (C) 28–280, and (D) 280–14,000 ppb obtained without (line a, blue color) and with (line b, red color) a 1 cm × 1 cm paper pad placed over the SPE under optimal experimental conditions.

**Effect Interferents and Long-Term Stability Analysis.** The selective detection of the sensor was investigated by introducing $Na^+$, $K^+$, $Ag^+$, $Cd^{2+}$, $Cu^{2+}$, $Hg^{2+}$, $Ca^{2+}$, $Mg^{2+}$, $Fe^{3+}$, $Co^{2+}$, $Ni^{2+}$, $Zn^{2+}$, and $Ba^{2+}$ individually and along with $Pb^{2+}$ and measuring the stripping peak potential at −0.63 V. The results (Table S4, Supporting Information) clearly show that the selective detection of $Pb^{2+}$ using sGO/PPy nanocomposite film was unaffected by the presence of these interfering metal ions. Figure 6 shows the results of 14 ppm $Pb^{2+}$ without (black line) and with low concentration of interferents (red line), namely, 0.15 ppm of $Cd^{2+}$, 0.2 ppm of $Cu^{2+}$, and 0.3 ppm of $Hg^{2+}$, and with high concentration of interferents (blue line), namely, 14 ppm of $Cd^{2+}$, $Cu^{2+}$, and $Hg^{2+}$ each. The DPASV peak current for $Pb^{2+}$ changed only minimally, from 63.1 (without interferents) to 64.9 and 66.6 μA, with low and high concentrations of interferents, respectively, with the peak potential shifting slightly from −0.63 to −0.71 V. This marginal change in the signal may be attributed to the formation of intermetallic compounds (Pb–Hg, Pb–Cu) during the deposition step.[55−57] However, the signal for $Pb^{2+}$ is much different from those for interfering metals, hence selective detection of $Pb^{2+}$ is unaffected.

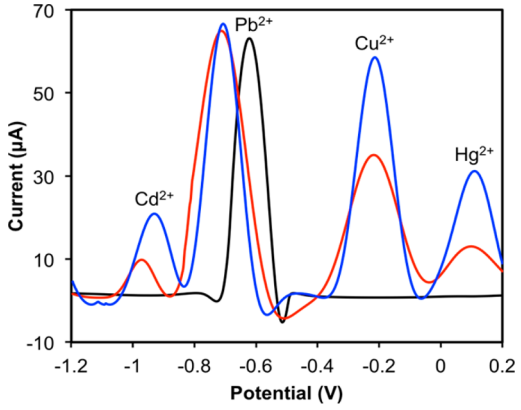


**Figure 6.** Typical DPASV (deposition potential = −1.2 V, deposition time =10 min) results of 14 ppm $Pb^{2+}$ at sGO/PPy-SPE in the absence (black line) and in the presence (red line) of 0.15 ppm of $Cd^{2+}$, 0.2 ppm of $Cu^{2+}$, and 0.3 ppm of $Hg^{2+}$ and (blue line) 14 ppm of $Cd^{2+}$, $Cu^{2+}$, and $Hg^{2+}$ each.

We also tested the effectiveness of our sensor for detecting $Pb^{2+}$ in spiked and real water samples of known and unknown $Pb^{2+}$ concentrations obtained from a local company. The data in Table 1 shows that the measured results are in good conformance with the expected values. The long-term stability of sGO/PPy-SPE is also very good. We investigated the detection of $Pb^{2+}$ in the range of 0.07–280 ppb for 30 days, measured at one-week intervals. The results show that the sensor response remained fairly constant over 30 days without

**Table 1. Analysis of $Pb^{2+}$ Content in Spiked and Industry Water Samples**

| sample | spiked (ppb) | ICP-MS[a] measurement (ppb) | sGO/PPy-SPE measurement (mean ± std. dev.) (ppb) |
|---|---|---|---|
| spiked 3 | 0.28 | N/A | 0.27 ± 0.014 |
| spiked 4 | 10 | N/A | 9.9 ± 0.118 |
| spiked 5 | 50 | N/A | 49.4 ± 2.9 |
| spiked 1 | 50 | N/A | 48.33 ± 3.5 |
| spiked 2 | 100 | N/A | 93.25 ± 7.6 |
| spiked 6 | 100 | N/A | 97.6 ± 4.1 |
| spiked 7 | 150 | N/A | 148.7 ± 3.2 |
| industry 1 | N/A | 3.96 | 3.28 ± 0.12 |
| industry 2 | N/A | – | 0.896 ± 0.03 |

[a]Inductively coupled plasma-mass spectrometry.


DOI: 10.1021/acsami.5b03904
ACS Appl. Mater. Interfaces 2015, 7, 15935–15943

any changes in anodic stripping peak potential (Table S5 and Figure S9, Supporting Information). The long-term performance of our sensor was compared with those of other similar sensors reported in the literature (Table S6, Supporting Information). As expected, the measurable detection limit changed from 0.07 to 0.28 ppb over 30 days, but it was much less compared to those of other potentiometric polymeric membrane−$Pb^{2+}$ selective electrode sensors.[13,58−60]

## CONCLUSIONS

We successfully synthesized sGO and electrochemically deposited the sGO/PPy nanocomposite film on the working electrode surface of SPE for highly sensitive detection of $Pb^{2+}$ in water. The developed nanocomposite film has good electron tunneling properties, large surface area, good conducting ability, high affinity to $Pb^{2+}$, and long-term stability. The sGO/PPy-SPE, when used without or with paper (for sample delivery), exhibited good sensitivity and high reproducibility. The fabricated $Pb^{2+}$ sensor is inexpensive, user-friendly, robust and reliable, requires only low-sample volume, and is unaffected by various interfering metal ions. In addition, the developed device can be used multiple times. Thus, our sGO/PPy-based $Pb^{2+}$ sensor holds great potential for the simultaneous detection of multiple toxic heavy metal ions in environmental, food, and biomedical samples.

## ASSOCIATED CONTENT

### Supporting Information

UV−vis absorption spectra, FT-IR spectra, wide scan XPS spectra, electrochemical polymerization, anodic stripping peak results, and long-term stability data. The Supporting Information is available free of charge on the ACS Publications website at DOI: 10.1021/acsami.5b03904.

## AUTHOR INFORMATION

### Corresponding Authors

*E-mail: wjchang@uwm.edu.
*E-mail: guna@wisc.edu.

### Notes

The authors declare no competing financial interest.

## ACKNOWLEDGMENTS

This work was financially supported by the U.S. National Science Foundation through the Industry/University Cooperative Research Center on Water Equipment & Policy located at the University of Wisconsin-Milwaukee (IIP-0968887) and Marquette University (IIP-0968844). Industry water samples were obtained from Pentair Ltd., and KX Technologies LLC. We also acknowledge the assistance of Yi-Cheng Wang in performing XPS, SEM, TEM characterizations and XPS analysis.

## REFERENCES

(1) World Health Organization. Biological Monitoring of Metals, 1994. http://apps.who.int/iris/bitstream/10665/62052/1/WHO_EHG_94.2.pdf.
(2) Jarup, L. Hazards of heavy metal contamination. *Br. Med. Bull.* **2003**, *68* (1), 167−182.
(3) Aragay, G.; Pons, J.; Merkoci, A. Recent trends in macro-, micro-, and nanomaterial-based tools and strategies for heavy-metal detection. *Chem. Rev.* **2011**, *111* (5), 3433−3458.
(4) Plumlee, G. S.; Durant, J. T.; Morman, S. A.; Neri, A.; Wolf, R. E.; Dooyema, C. A.; Hageman, P. L.; Lowers, H. A.; Fernette, G. L.; Meeker, G. P.; Benzel, W. M.; Driscoll, R. L.; Berry, C. J.; Crock, J. G.; Goldstein, H. L.; Adams, M.; Bartrem, C. L.; Tirima, S.; Behbod, B.; von Lindern, I.; Brown, M. J. Linking geological and health sciences to assess childhood lead poisoning from artisanal gold mining in Nigeria. *Environ. Health Perspect.* **2013**, *121* (6), 744−750.
(5) Navas-Acien, A.; Guallar, E.; Silbergeld, E. K.; Rothenberg, S. J. Lead exposure and cardiovascular disease–a systematic review. *Environ. Health Perspect.* **2007**, *115* (3), 472−482.
(6) World Health Organization. Guidelines for Drinking-Water Quality, 4th ed., 2011. http://whqlibdoc.who.int/publications/2011/9789241548151_eng.pdf.
(7) U.S. Environmental Protection Agency. Basic Information about Lead in Drinking Water, 2015. http://water.epa.gov/drink/contaminants/basicinformation/lead.cfm (accessed March 9, 2015).
(8) Li, Z.; Chen, J.; Liu, M.; Yang, Y. Supramolecular solvent-based microextraction of copper and lead in water samples prior to reacting with synthesized Schiff base by flame atomic absorption spectrometry determination. *Anal. Methods* **2014**, *6* (7), 2294−2298.
(9) Zougagh, M.; Garcia de Torres, A.; Vereda Alonso, E.; Cano Pavon, J. M. Automatic on line preconcentration and determination of lead in water by ICP-AES using a TS-microcolumn. *Talanta* **2004**, *62* (3), 503−510.
(10) Suleiman, J. S.; Hu, B.; Huang, C.; Zhang, N. Determination of Cd, Co, Ni and Pb in biological samples by microcolumn packed with black stone (Pierre noire) online coupled with ICP-OES. *J. Hazard. Mater.* **2008**, *157* (2−3), 410−417.
(11) Su, S.; Chen, B.; He, M.; Hu, B. Graphene oxide-silica composite coating hollow fiber solid phase microextraction online coupled with inductively coupled plasma mass spectrometry for the determination of trace heavy metals in environmental water samples. *Talanta* **2014**, *123*, 1−9.
(12) Izumi, Y.; Kiyotaki, F.; Minato, T.; Seida, Y. X-ray absorption fine structure combined with fluorescence spectrometry for monitoring trace amounts of lead adsorption in the environmental conditions. *Anal. Chem.* **2002**, *74* (15), 3819−3823.
(13) Huang, M. R.; Ding, Y. B.; Li, X. G.; Liu, Y. J.; Xi, K.; Gao, C. L.; Kumar, R. V. Synthesis of Semiconducting Polymer Microparticles as Solid Ionophore with Abundant Complexing Sites for Long-Life Pb(II) Sensors. *ACS Appl. Mater. Interfaces* **2014**, *6* (24), 22096−22107.
(14) Rahman, M. A.; Won, M. S.; Shim, Y. B. Characterization of an EDTA bonded conducting polymer modified electrode: its application for the simultaneous determination of heavy metal ions. *Anal. Chem.* **2003**, *75* (5), 1123−1129.
(15) Wei, Y.; Yang, R.; Liu, J. H.; Huang, X. J. Selective detection toward Hg(II) and Pb(II) using polypyrrole/carbonaceous nanospheres modified screen-printed electrode. *Electrochim. Acta* **2013**, *105*, 218−223.
(16) Rajesh, S.; Kanugula, A. K.; Bhargava, K.; Ilavazhagan, G.; Kotamraju, S.; Karunakaran, C. Simultaneous electrochemical determination of superoxide anion radical and nitrite using Cu,ZnSOD immobilized on carbon nanotube in polypyrrole matrix. *Biosens. Bioelectron.* **2010**, *26* (2), 689−695.
(17) Yang, J.; Yu, J. H.; Rudi Strickler, J.; Chang, W. J.; Gunasekaran, S. Nickel nanoparticle-chitosan-reduced graphene oxide-modified screen-printed electrodes for enzyme-free glucose sensing in portable microfluidic devices. *Biosens. Bioelectron.* **2013**, *47*, 530−538.
(18) Yang, J.; Nam, Y. G.; Lee, S. K.; Kim, C. S.; Koo, Y. M.; Chang, W. J.; Gunasekaran, S. Paper-fluidic electrochemical biosensing platform with enzyme paper and enzymeless electrodes. *Sens. Actuators, B* **2014**, *203*, 44−53.
(19) Li, J.; Guo, S.; Zhai, Y.; Wang, E. Nafion-graphene nanocomposite film as enhanced sensing platform for ultrasensitive determination of cadmium. *Electrochem. Commun.* **2009**, *11* (5), 1085−1088.
(20) Morton, J.; Havens, N.; Mugweru, A.; Wanekaya, A. K. Detection of Trace Heavy Metal Ions Using Carbon Nanotube-Modified Electrodes. *Electroanalysis* **2009**, *21* (14), 1597−1603.


DOI: 10.1021/acsami.5b03904
*ACS Appl. Mater. Interfaces* 2015, 7, 15935−15943

(21) Chen, L.; Su, Z.; He, X.; Liu, Y.; Qin, C.; Zhou, Y.; Li, Z.; Wang, L.; Xie, Q.; Yao, S. Square wave anodic stripping voltammetric determination of Cd and Pb ions at a Bi/Nafion/thiolated polyaniline/glassy carbon electrode. *Electrochem. Commun.* **2012**, *15* (1), 34−37.
(22) Zhao, Z. Q.; Chen, X.; Yang, Q.; Liu, J. H.; Huang, X. J. Selective adsorption toward toxic metal ions results in selective response: electrochemical studies on a polypyrrole/reduced graphene oxide nanocomposite. *Chem. Commun.* **2012**, *48* (16), 2180−2182.
(23) Wang, J.; Bian, C.; Tong, J.; Sun, J.; Xia, S. L-Aspartic acid/L-cysteine/gold nanoparticle modified microelectrode for simultaneous detection of copper and lead. *Thin Solid Films* **2012**, *520* (21), 6658−6663.
(24) Zhou, H.; Wang, X.; Yu, P.; Chen, X.; Mao, L. Sensitive and selective voltammetric measurement of Hg2+ by rational covalent functionalization of graphene oxide with cysteamine. *Analyst* **2012**, *137* (2), 305−308.
(25) Fu, X. C.; Wu, J.; Li, J.; Xie, C. G.; Liu, Y. S.; Zhong, Y.; Liu, J. H. Electrochemical determination of trace copper(II) with enhanced sensitivity and selectivity by gold nanoparticle/single-wall carbon nanotube hybrids containing three-dimensional L-cysteine molecular adapters. *Sens. Actuators, B* **2013**, *182*, 382−389.
(26) Zhang, J. T.; Jin, Z. Y.; Li, W. C.; Dong, W.; Lu, A. H. Graphene modified carbon nanosheets for electrochemical detection of Pb(II) in water. *J. Mater. Chem. A* **2013**, *1* (42), 13139−13145.
(27) Gong, X.; Bi, Y.; Zhao, Y.; Liu, G.; Teoh, W. Y. Graphene oxide-based electrochemical sensor: a platform for ultrasensitive detection of heavy metal ions. *RSC Adv.* **2014**, *4* (47), 24653−24657.
(28) Zhu, L.; Xu, L.; Huang, B.; Jia, N.; Tan, L.; Yao, S. Simultaneous determination of Cd(II) and Pb(II) using square wave anodic stripping voltammetry at a gold nanoparticle-graphene-cysteine composite modified bismuth film electrode. *Electrochim. Acta* **2014**, *115*, 471−477.
(29) Muralikrishna, S.; Sureshkumar, K.; Varley, T. S.; Nagaraju, D. H.; Ramakrishnappa, T. In situ reduction and functionalization of graphene oxide with L-cysteine for simultaneous electrochemical determination of cadmium(II), lead(II), copper(II), and mercury(II) ions. *Anal. Methods* **2014**, *6* (21), 8698−8705.
(30) Yan, X.; Chen, J.; Yang, J.; Xue, Q.; Miele, P. Fabrication of free-standing, electrochemically active, and biocompatible graphene oxide-polyaniline and graphene-polyaniline hybrid papers. *ACS Appl. Mater. Interfaces* **2010**, *2* (9), 2521−2529.
(31) Choi, M.; Jang, J. Heavy metal ion adsorption onto polypyrrole-impregnated porous carbon. *J. Colloid Interface Sci.* **2008**, *325* (1), 287−289.
(32) Tolani, S.; Mugweru, A.; Craig, M.; Wanekaya, A. K. Rapid and Efficient Removal of Heavy Metal Ions from Aqueous Media Using Cysteine-Modified Polymer Nanowires. *J. Appl. Polym. Sci.* **2010**, *116* (1), 308−313.
(33) Hummers, W. S.; Offeman, R. E. Preparation of Graphitic Oxide. *J. Am. Chem. Soc.* **1958**, *80* (6), 1339−1339.
(34) Cote, L. J.; Kim, F.; Huang, J. Langmuir-Blodgett assembly of graphite oxide single layers. *J. Am. Chem. Soc.* **2009**, *131* (3), 1043−1049.
(35) Park, S.; Ruoff, R. S. Chemical methods for the production of graphenes. *Nat. Nanotechnol.* **2009**, *4* (4), 217−224.
(36) Eda, G.; Chhowalla, M. Chemically derived graphene oxide: towards large-area thin-film electronics and optoelectronics. *Adv. Mater.* **2010**, *22* (22), 2392−2415.
(37) Shen, J.; Yan, B.; Shi, M.; Ma, H.; Li, N.; Ye, M. Synthesis of graphene oxide-based biocomposites through diimide-activated amidation. *J. Colloid Interface Sci.* **2011**, *356* (2), 543−549.
(38) Mousavi, M. F.; Rahmani, A.; Golabi, S. M.; Shamsipur, M.; Sharghi, H. Differential pulse anodic stripping voltammetric determination of lead(II) with a 1,4-bis(prop-2′-enyloxy)-9,10-anthraquinone modified carbon paste electrode. *Talanta* **2001**, *55* (2), 305−312.
(39) Ramesha, G. K.; Sampath, S. Exfoliated graphite oxide modified electrode for the selective determination of picomolar concentration of lead. *Electroanalysis* **2007**, *19* (23), 2472−2478.
(40) Luo, Z.; Lu, Y.; Somers, L. A.; Johnson, A. T. C. High yield preparation of macroscopic graphene oxide membranes. *J. Am. Chem. Soc.* **2009**, *131* (3), 898−899.
(41) Chen, D.; Li, L.; Guo, L. An environment-friendly preparation of reduced graphene oxide nanosheets via amino acid. *Nanotechnology* **2011**, *22* (32), 325601.
(42) Liu, Z.; Jiang, L.; Galli, F.; Nederlof, I.; Olsthoorn, R. C. L.; Lamers, G. E. M.; Oosterkamp, T. H.; Abrahams, J. P. A Graphene Oxide center dot Streptavidin Complex for Biorecognition - Towards Affinity Purification. *Adv. Funct. Mater.* **2010**, *20* (17), 2857−2865.
(43) Yang, T.; Liu, L. H.; Liu, J. W.; Chen, M. L.; Wang, J. H. Cyanobacterium metallothionein decorated graphene oxide nanosheets for highly selective adsorption of ultra-trace cadmium. *J. Mater. Chem.* **2012**, *22* (41), 21909−21916.
(44) Aryal, S.; Remant, B. K. C.; Dharmaraj, N.; Bhattarai, N.; Kim, C. H.; Kim, H. Y. Spectroscopic identification of S-Au interaction in cysteine capped gold nanoparticles. *Spectrochim. Acta, Part A* **2006**, *63* (1), 160−163.
(45) Ortolani, L.; Cadelano, E.; Veronese, G. P.; Boschi, C. D. E.; Snoeck, E.; Colombo, L.; Morandi, V. Folded Graphene Membranes: Mapping Curvature at the Nanoscale. *Nano Lett.* **2012**, *12* (10), 5207−5212.
(46) Zhu, C.; Zhai, J.; Wen, D.; Dong, S. Graphene oxide/polypyrrole nanocomposites: one-step electrochemical doping, coating and synergistic effect for energy storage. *J. Mater. Chem.* **2012**, *22* (13), 6300−6306.
(47) Ye, D.; Luo, L.; Ding, Y.; Chen, Q.; Liu, X. A novel nitrite sensor based on graphene/polypyrrole/chitosan nanocomposite modified glassy carbon electrode. *Analyst* **2011**, *136* (21), 4563−4569.
(48) Wei, Y.; Yang, R.; Zhang, Y. X.; Wang, L.; Liu, J. H.; Huang, X. J. High adsorptive gamma-AlOOH(boehmite)@SiO2/Fe3O4 porous magnetic microspheres for detection of toxic metal ions in drinking water. *Chem. Commun.* **2011**, *47* (39), 11062−11064.
(49) Nie, Z.; Nijhuis, C. A.; Gong, J.; Chen, X.; Kumachev, A.; Martinez, A. W.; Narovlyansky, M.; Whitesides, G. M. Electrochemical sensing in paper-based microfluidic devices. *Lab Chip* **2010**, *10* (4), 477−483.
(50) Cate, D. M.; Adkins, J. A.; Mettakoonpitak, J.; Henry, C. S. Recent Developments in Paper-Based Microfluidic Devices. *Anal. Chem.* **2015**, *87* (1), 19−41.
(51) Yantasee, W.; Lin, Y.; Zemanian, T. S.; Fryxell, G. E. Voltammetric detection of lead(II) and mercury(II) using a carbon paste electrode modified with thiol self-assembled monolayer on mesoporous silica (SAMMS). *Analyst* **2003**, *128* (5), 467−472.
(52) Philips, M. F.; Gopalan, A. I.; Lee, K. P. Development of a novel cyano group containing electrochemically deposited polymer film for ultrasensitive simultaneous detection of trace level cadmium and lead. *J. Hazard. Mater.* **2012**, *237*−*238*, 46−54.
(53) Tan, S. N.; Ge, L.; Wang, W. Paper Disk on Screen Printed Electrode for One-Step Sensing with an Internal Standard. *Anal. Chem.* **2010**, *82* (21), 8844−8847.
(54) Feng, Q. M.; Zhang, Q.; Shi, C. G.; Xu, J. J.; Bao, N.; Gu, H. Y. Using nanostructured conductive carbon tape modified with bismuth as the disposable working electrode for stripping analysis in paper-based analytical devices. *Talanta* **2013**, *115*, 235−240.
(55) Schiewe, J.; Oldham, K. B.; Myland, J. C.; Bond, A. M.; Vicente-Beckett, V. A.; Fletcher, S. Linear-scan anodic stripping voltammetry with thin-film electrodes: Theory of the stripping stage and experimental tests. *Anal. Chem.* **1997**, *69* (14), 2673−2681.
(56) Tibbetts, D. F.; Davis, J.; Compton, R. G. Sonoelectroanalytical detection of lead at a bare copper electrode. *Fresenius' J. Anal. Chem.* **2000**, *368* (4), 412−414.
(57) Wei, Y.; Gao, C.; Meng, F. L.; Li, H. H.; Wang, L.; Liu, J. H.; Huang, X. J. SnO2/Reduced Graphene Oxide Nanocomposite for the Simultaneous Electrochemical Detection of Cadmium(II), Lead(II), Copper(II), and Mercury(II): An Interesting Favorable Mutual Interference. *J. Phys. Chem. C* **2012**, *116* (1), 1034−1041.
(58) Ceresa, A.; Bakker, E.; Hattendorf, B.; Gunther, D.; Pretsch, E. Potentiometric polymeric membrane electrodes for measurement of


DOI: 10.1021/acsami.5b03904
*ACS Appl. Mater. Interfaces* 2015, 7, 15935−15943

environmental samples at trace levels: New requirements for selectivities and measuring protocols, and comparison with ICPMS. *Anal. Chem.* **2001**, *73* (2), 343−351.
(59) Mazloum-Ardakani, M.; Safari, J.; Pourhakkak, P.; Sheikh-Mohseni, M. A. Determination of lead (II) ion by highly selective and sensitive lead (II) membrane electrode based on 2-(((E)-2-((E)-1-(2-hydroxyphenyl)methyliden)hydrazono)metyl)phenol. *Int. J. Environ. Anal. Chem.* **2012**, *92* (14), 1638−1649.
(60) Rouhollahi, A.; Reza Ganjali, M.; Shamsipur, M. Lead ion selective PVC membrane electrode based on 5,5′-dithiobis-(2-nitrobenzoic acid). *Talanta* **1998**, *46* (6), 1341−1346.


DOI: 10.1021/acsami.5b03904
*ACS Appl. Mater. Interfaces* 2015, 7, 15935−15943